Commun. Comput. Phys.
doi: 10.4208/cicp.2009.09.042

Vol. **7**, No. 3, pp. 403-422
March 2010

Stick-Slip Motion of Moving Contact Line on Chemically Patterned Surfaces

Congmin Wu[1], Siulong Lei[1], Tiezheng Qian[2,*] and Xiaoping Wang[2]

[1] *Department of Mathematics, Hong Kong University of Science and Technology, Clear Water Bay, Kowloon, Hong Kong.*
[2] *Department of Mathematics and Joint KAUST-HKUST Micro/Nano-Fluidics Laboratory, Hong Kong University of Science and Technology, Clear Water Bay, Kowloon, Hong Kong.*

Received 27 February 2009; Accepted (in revised version) 16 July 2009

Available online 1 September 2009

Abstract. Based on our continuum hydrodynamic model for immiscible two-phase flows at solid surfaces, the stick-slip motion has been predicted for moving contact line at chemically patterned surfaces [Wang et al., J. Fluid Mech., 605 (2008), pp. 59-78]. In this paper we show that the continuum predictions can be quantitatively verified by molecular dynamics (MD) simulations. Our MD simulations are carried out for two immiscible Lennard-Jones fluids confined by two planar solid walls in Poiseuille flow geometry. In particular, one solid surface is chemically patterned with alternating stripes. For comparison, the continuum model is numerically solved using material parameters directly measured in MD simulations. From oscillatory fluid-fluid interface to intermittent stick-slip motion of moving contact line, we have quantitative agreement between the continuum and MD results. This agreement is attributed to the accurate description down to molecular scale by the generalized Navier boundary condition in our continuum model. Numerical results are also presented for the relaxational dynamics of fluid-fluid interface, in agreement with a theoretical analysis based on the Onsager principle of minimum energy dissipation.

PACS: 68.08.-p, 83.50.Rp, 83.10.Mj, 83.10.Ff

Key words: Moving contact line, slip boundary condition, patterned surface.

1 Introduction

The contact line denotes the intersection of the fluid-fluid interface with the solid wall in immiscible two-phase flows. When one fluid displaces the other, the contact line moves

*Corresponding author. *Email addresses:* macmin@ust.hk (C. Wu), malsl@ust.hk (S. Lei), maqian@ust.hk (T. Qian), mawang@ust.hk (X. Wang)

along the wall. As a classical problem in continuum hydrodynamics, it has been known for decades that the moving contact line is incompatible with the no-slip boundary condition [1] — the latter leads to a non-integrable singularity in viscous dissipation [2–4]. In particular, molecular dynamics (MD) simulations have shown that near-complete slip indeed occurs at the moving contact line [5, 6]. Numerous models were proposed to address this problem, but none was able to give a quantitative account of the MD slip velocity in the molecular-scale vicinity of the contact line [7–15].

Through analysis of extensive MD data, it was discovered that the slip velocity measured in nanoscale MD simulations satisfies the generalized Navier boundary condition (GNBC) [16]. The GNBC states that the relative slip velocity between the fluid and the solid wall is proportional to the total tangential stress — the sum of the viscous stress and the uncompensated Young stress; the latter arises from the deviation of the fluid-fluid interface from its static configuration. By the use of the Cahn-Hilliard (CH) hydrodynamic formulation for two-phase flows [13, 14, 17], the implementation of the GNBC leads to continuum solutions in quantitative agreement with MD simulation results [16, 18, 19]. Recently, it has been shown [20, 21] that the GNBC can be derived in a variational approach from the Onsager principle of minimum energy dissipation [22, 23].

Recently, structured surfaces exhibiting lateral patterns of varying wettability have become technically available. The morphologies of liquid on patterned surfaces with hydrophilic and hydrophobic regions have been investigated experimentally and theoretically [24,25]. While the statics of wetting on patterned surfaces already leads to a large variety of morphologies, the dynamics of wetting on these surfaces is even more complicated. Cubaud and Fermigier carried out an experimental investigation on the advancing contact lines of large drops spreading on chemically patterned surfaces [26]. In a numerical study for an immiscible two-phase fluid driven to flow past chemically patterned surfaces in a microchannel, Kuksenok *et al*. showed that the fluid exhibits morphological instabilities giving rise to the formation of monodisperse droplets of one phase in the other phase [27]. Through both numerical simulations and experiments, Kusumaatmaja *et al*. explored the behavior of liquid drops moving past a surface patterned with hydrophobic and hydrophilic stripes [28].

We would like to point out that in all the previous studies based on diffuse-interface modeling [12–15, 27, 28], the no-slip boundary condition is kept and the non-integrable stress singularity is removed by introducing diffusive transport through the fluid-fluid interface. By combining the GNBC with the diffuse-interface formulation, our continuum model allows the coexistence of slip and diffusion, with their competition determined by the relative magnitudes of relevant parameters [20]. For the systems simulated in our MD study, it is the slip that dominates. A recent study by Ren and E [29], which focused on a sharp interface model, also demonstrated that the stress singularity is regularized by the existence of a slip region and the Young stress is dominant in the contact line region. We have applied our model to further investigate the role of slip for contact line motion at surfaces patterned with stripes of varying contact angle [30]. We found that as the fluid-fluid interface is displaced along the patterned surface, its shape is periodically

adjusted by the underlying pattern and the contact line undergoes a stick-slip movement with an oscillatory slip velocity. Such an oscillatory movement leads to extra dissipation, for which a scaling relation was found in the limit of slow displacement.

The purpose of this paper is to demonstrate that the continuum predictions in [30] can be quantitatively verified by MD simulations. Our MD simulations are carried out for two immiscible Lennard-Jones fluids confined by two planar solid walls in Poiseuille flow geometry. In particular, one solid surface is chemically patterned with alternating stripes. For comparison, the continuum model is numerically solved using material parameters directly measured in MD simulations. From the oscillatory fluid-fluid interface to the intermittent stick-slip motion of contact line, we have quantitative agreement between the continuum and MD results. This agreement is attributed to the accurate description down to molecular scale by the GNBC. Numerical results are also presented for the relaxational dynamics of fluid-fluid interface, in agreement with a theoretical analysis based on the variational principle of Onsager.

The paper is organized as follows. In Section 2 the continuum hydrodynamic model is introduced for contact line motion at chemically patterned surfaces. In Section 3 the MD simulations are outlined for the systems modeled in our continuum formulation. The technical details for continuum calculations are presented in Section 4, together with the challenge we meet in making comparison of continuum and MD results. The numerical results are presented in Section 5. The stick-slip motion of moving contact line is observed with remarkable agreement between the continuum and MD results. The relaxational dynamics of fluid-fluid interface is investigated numerically and theoretically. The paper is concluded in Section 6 with some remarks.

2 Continuum hydrodynamic model

2.1 Modeling moving contact line

From numerical simulation to theoretical formulation, recent evidences have shown that the GNBC can quantitatively account for the slip velocity measured in MD simulations [16, 18, 20]. The GNBC has been combined with the Cahn-Hilliard (CH) free energy [17] to formulate a phase-field description of immiscible two-phase flows. Below we briefly present the continuum hydrodynamic model which is capable of not only reproducing MD results but also simulating contact-line motion on a scale much larger than that accessible by MD simulations [18].

The CH free energy functional is of the form

$$F[\phi]=\int d\mathbf{r}\left[\frac{K}{2}(\nabla\phi)^2+f(\phi)\right], \tag{2.1}$$

introduced to energetically stabilize the diffuse fluid-fluid interface between the two immiscible fluid phases. Here $\phi(\mathbf{r})$ is the phase field, locally defined from $\phi=(\rho_2-\rho_1)/(\rho_2+$

ρ_1), with ρ_1 and ρ_2 being the local number densities of the two fluid phases;

$$f(\phi)=-r\phi^2/2+u\phi^4/4,$$

in which K, r, and u are parameters that can be determined from the characteristic interfacial thickness $\xi=\sqrt{K/r}$, the interfacial tension $\gamma=2\sqrt{2}r^2\xi/3u$, and the two homogeneous equilibrium phases

$$\phi_\pm=\pm\sqrt{r/u}\ \ (=\pm 1 \text{ here}),$$

all being measurable quantities in MD simulations. To determine ξ, the normalized density difference between the two immiscible fluids is measured in MD simulations and then fitted by $\tanh[(x-x_0)/\sqrt{2}\xi]$, the profile minimizing the Cahn-Hilliard free energy (for a flat interface parallel to the yz plane and centered at x_0), as shown in Fig. 1. The value of γ is measured in MD simulations by integrating the stress anisotropy across the fluid-fluid interface along the interface normal. The two coupled equations of motion are the convection-diffusion equation for $\phi(\mathbf{r})$ and the Navier-Stokes equation in the presence of the capillary force:

$$\frac{\partial\phi}{\partial t}+\mathbf{v}\cdot\nabla\phi=M\nabla^2\mu, \tag{2.2}$$

$$\rho_m\left[\frac{\partial\mathbf{v}}{\partial t}+(\mathbf{v}\cdot\nabla)\mathbf{v}\right]=-\nabla p+\nabla\cdot\boldsymbol{\sigma}^v+\mu\nabla\phi+\mathbf{f}_e, \tag{2.3}$$

together with the incompressibility condition $\nabla\cdot\mathbf{v}=0$. Here $\mu=-K\nabla^2\phi-r\phi+u\phi^3(=\delta F/\delta\phi)$ is the chemical potential, M is the mobility coefficient, ρ_m is the mass density of the fluid, p is the pressure, $\boldsymbol{\sigma}^v=\eta\left[(\nabla\mathbf{v})+(\nabla\mathbf{v})^T\right]$ is the Newtonian viscous stress tensor with η being the viscosity, $\mu\nabla\phi$ is the capillary force density, and $\mathbf{f}_e$ is the external force density. The boundary conditions at the solid surface are the kinematic impermeability conditions $\partial_n\mu=0$, $v_n=0$, the dynamic relaxational equation for ϕ at surface:

$$\frac{\partial\phi}{\partial t}+v_\tau\partial_\tau\phi=-\Gamma L(\phi), \tag{2.4}$$

and the GNBC governing the fluid slip at solid surface:

$$\beta(\phi)v_\tau^{slip}=-\eta(\partial_n v_\tau+\partial_\tau v_n)+L(\phi)\partial_\tau\phi. \tag{2.5}$$

Here τ denotes the direction tangent to the solid surface (for two-dimensional flows), n denotes the outward pointing surface normal, Γ is a positive phenomenological parameter, $L(\phi)=K\partial_n\phi+\partial\gamma_{fs}(\phi)/\partial\phi$ with $\gamma_{fs}(\phi)$ being the fluid-solid interfacial free energy per unit area, $\beta(\phi)$ is the slip coefficient which may locally depend on ϕ at surface, and $L(\phi)\partial_\tau\phi$ is the uncompensated Young stress. The slip length is locally defined as $l_s(\phi)=\eta/\beta(\phi)$. We use

$$\gamma_{fs}(\phi)=(\Delta\gamma_{fs}/2)\sin(\pi\phi/2)$$

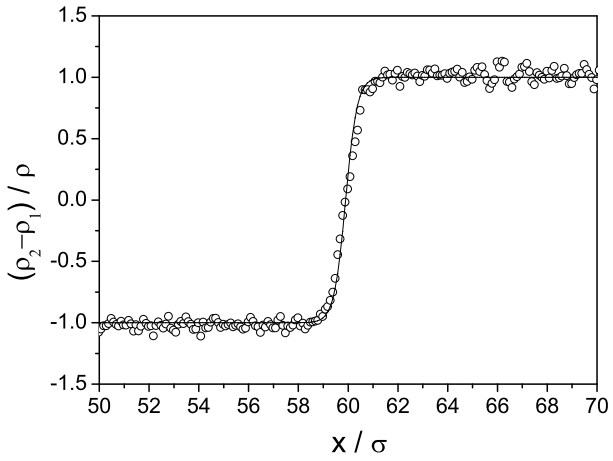

Figure 1: The normalized density difference between the two immiscible fluids $(\rho_2-\rho_1)/\rho$ is plotted as a function of x along the interfacial normal. The interface is parallel to the yz plane and centered at $x_0=59.9\sigma$. It is seen that the MD profile (circles) is well fitted by $\tanh[(x-x_0)/\sqrt{2}\xi]$ with $\xi=0.33\sigma$ (solid line). Here σ is the range parameter in the Lennard-Jones potential for fluid-fluid interactions (see Section 3 for details). The system in MD simulation is large enough to avoid any undesired boundary effects on interfacial profile. The data are collected from bins that measure 0.1σ along x, 9.0σ along y, and 1.0σ along z. Time averaging has been used to reduce the statistical fluctuations (which can be further reduced by longer time averaging).

which is a smooth interpolation from $\gamma_{fs}(\phi_-)=-\Delta\gamma_{fs}/2$ to $\gamma_{fs}(\phi_+)=\Delta\gamma_{fs}/2$. According to the Young's equation for the static contact angle θ_s:

$$\gamma_{fs}(\phi_+)+\gamma\cos\theta_s=\gamma_{fs}(\phi_-),$$

we have $\Delta\gamma_{fs}=-\gamma\cos\theta_s$. In the sharp interface limit [16, 31], the uncompensated Young stress satisfies

$$\int_{int} d\tau[L(\phi)\partial_\tau\phi]=\gamma(\cos\theta_d-\cos\theta_s), \tag{2.6}$$

where $\int_{int}d\tau$ denotes the integration across the fluid-fluid interface along the τ direction and θ_d is the dynamic contact angle. Physically, it is clear that the uncompensated Young stress arises from the deviation of the fluid-fluid interface from its static configuration.

We want to point out that in "standard" diffuse-interface model(s), the no slip condition is applied and the stress singularity is relaxed/removed by diffusion only. In our diffuse-interface model, however, the diffusion mechanism is kept and the slip mechanism is added through the application of the GNBC. The two mechanisms coexist in the model and the relative importance of each can be tuned by the relevant physical parameter (the mobility coefficient M or the slip coefficient β). There can be two extreme cases, one with diffusion only and the other with slip only. The difference between these two extremes is qualitative in terms of the flow field in the close vicinity of the moving contact line. (If there is diffusion only, then the relevant length scale is the diffusion length $l_d=\sqrt{M\eta}$. If there is slip only, then the relevant length scale is the slip length $l_s=\eta/\beta$.)

We want to emphasize that in modeling the systems in our MD simulations, diffusion is considered negligible while slip is dominant.

2.2 Modeling chemically patterned surfaces

We consider a two-phase fluid flowing through a two-dimensional channel (a slit pore) in which the top surface is homogeneous (labeled by c) while the bottom surface is chemically patterned. The two-phase fluid consists of two immiscible phases A and B. The bottom surface is patterned by the A-like and B-like stripes, labeled by a and b respectively. The A phase is more attracted to the A-like stripe than the B phase is while the B phase is more attracted to the B-like stripe than the A phase is, as illustrated in Fig. 2. The properties of each stripe are specified by a static contact angle (defined on the side of the B phase): θ_s^a at the A-like stripe (a) or θ_s^b at the B-like stripe (b), and two slip lengths: l_{sA}^a and l_{sB}^a at the A-like stripe or l_{sA}^b and l_{sB}^b at the B-like stripe for the two phases. To reduce the number of independent parameters, we further assume $\theta_s^b = 180^o - \theta_s^a$ (with $\theta_s^b < 90^o$), $l_{sA}^a = l_{sB}^b$, and $l_{sA}^b = l_{sB}^a$. Physically, larger slip length is associated with less wetting, i.e., less attractive fluid-solid interaction [32]. Therefore, we use $l_{sA}^a < l_{sA}^b$.

For an inhomogeneous patterned surface, the static contact angle and slip lengths appear in the continuum model as locally defined phenomenological material parameters. For the patterned surfaces consider here, each of these parameters varies as a step function across the stripe boundary. In general, the patterning may be modeled by other oscillating behaviors. In the study of single-phase flow past a chemically patterned surface [33–38], we have shown through both MD and continuum simulations that the slip length can be locally defined for a continuum hydrodynamic description as long as the fluid-solid interaction does not change too fast compared to the pattern period [38]. Physically, a continuum hydrodynamic model describes those variations hat are slow in both space and time and the parameters involved in such model can be locally defined in a coarse-grained sense.

3 Molecular dynamics simulations

MD simulations have been performed for two immiscible fluids confined in a slit pore by two planar solid walls parallel to the xy plane (see Fig. 3). The top wall has a homogeneous surface at $z = H$ and the bottom wall has a patterned surface at $z = 0$. Each wall is constructed by two [001] planes of an fcc lattice, with each molecule attached to a lattice site by a harmonic spring. The two fluids are labeled by A and B, respectively, and the top wall is labeled by c. The bottom wall is periodically patterned with the stripes formed by A-like and B-like solid molecules, labeled by a and b. The A-like and B-like stripes are of widths λ_a and λ_b as already set in the continuum model. The dimension of MD simulation box in the x direction is set as an integral multiple of the pattern period $\lambda = \lambda_a + \lambda_b$.

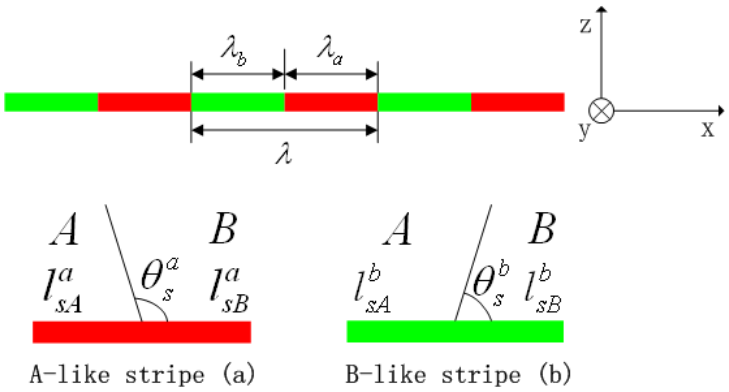

Figure 2: Schematic illustration for the chemically patterned surface with alternating A-like and B-like stripes. Each stripe is characterized by a contact angle and two slip lengths. The A-like and B-like stripes are of widths λ_a and λ_b and the patterning period is $\lambda=\lambda_a+\lambda_b$.

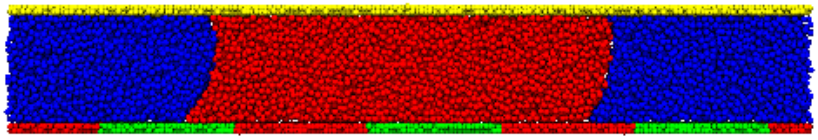

Figure 3: MD simulation sample for the immiscible Poiseuille flows. The colored symbols indicate the instantaneous molecular positions projected onto the xz plane. Here the fluid A is blue, the fluid B is red, the solid a is red, the solid b is green, and the solid c is yellow. The fluid B appears to be sandwiched by the fluid A due to the periodic boundary condition along the x direction. While there are two fluid-fluid interfaces, we collect the data for the one with the fluid B right to the fluid A.

In our MD simulations, interaction between any two molecules separated by distance r is modeled by a modified Lennard-Jones potential $U_{\alpha\beta}(r)=4\epsilon_{\alpha\beta}[(\sigma_{\alpha\beta}/r)^{12}-\delta_{\alpha\beta}(\sigma_{\alpha\beta}/r)^6]$, where the subscriptions α and β denote the molecule species, i.e., A, B, a, b, and c. The energy parameters $\epsilon_{\alpha\beta}$ and the range parameters $\sigma_{\alpha\beta}$ for fluid-fluid interactions are given by ϵ and σ, respectively, while those for fluid-solid interactions are given by 1.16ϵ and 1.04σ, respectively. Here ϵ and σ are the energy and length scales for all the intermolecular interactions. The dimensionless parameter $\delta_{\alpha\beta}$ is introduced to ensure the immiscibility between the different fluids and also to modify the wetting property of each fluid as well. We use $\delta_{AA}=\delta_{BB}=1$ for fluid molecules of the same species, $\delta_{AB}=\delta_{BA}=-1$ to ensure the immiscibility between the two fluids, and $\delta_{Aa}>\delta_{Ba}>0$ and $\delta_{Bb}>\delta_{Ab}>0$ for fluid-solid interactions. The last two expressions mean that the fluid A is more attracted to the A-like stripe than the fluid B is while the fluid B is more attracted to the B-like stripe than the fluid A is. To reduce the number of independent parameters, we further assume $\delta_{Aa}=\delta_{Bb}$ and $\delta_{Ab}=\delta_{Ba}$. The two fluids have the same interaction with the top wall, and hence $\delta_{Ac}=\delta_{Bc}$. The mass of each fluid molecule and that of each wall molecule are both m. The average number density of fluid molecules is $\rho=0.81\sigma^{-3}$ while the number density of wall molecules is $\rho_w=1.86\sigma^{-3}$. The temperature is controlled at $1.4\epsilon/k_B$ by the Langevin

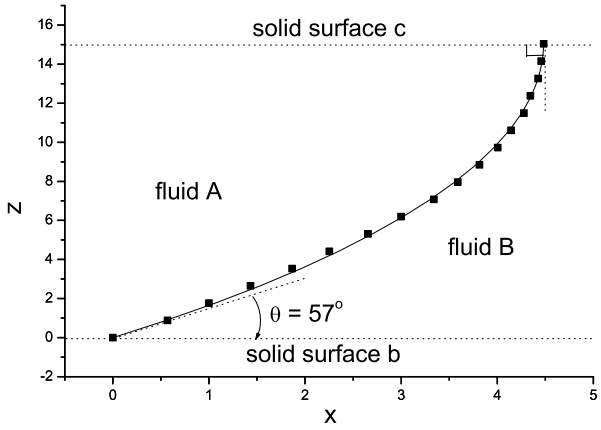

Figure 4: The fluid-fluid interface is located by the condition $\rho_1=\rho_2$, i.e., $\phi=0$. By fitting the static interface (squares) using a circular arc (solid line, with a 90^o contact angle at the top surface), the static contact angle at the A-like or B-like stripe can be determined. Shown here is the fluid-fluid interface between the solid surfaces b (bottom) and c (top), from which the static contact angle $\theta_s^b=57^o$ is determined. Parameters used are $\delta_{Aa}=\delta_{Bb}=\delta_{Ac}=\delta_{Bc}=0.7$ and $\delta_{Ab}=\delta_{Ba}=0.2$.

thermostat, where k_B is Boltzmann constant. The equations of motion are integrated using the velocity Verlet algorithm with a time step $\Delta t=0.001\tau$ where $\tau=\sqrt{m\sigma^2/\epsilon}$. The interaction potential $U_{\alpha\beta}$ is cut off at $r_c=2.5\sigma$. Periodic boundary conditions are imposed in the x and y directions. As a consequence, there is always one fluid sandwiched by the other fluid along the x direction.

To simulate the immiscible two-phase Poiseuille flows, a body force $mg\hat{\mathbf{x}}$ is applied to each fluid molecule in the x direction. In our simulations, the two fluids are separated by a clear interface while flowing past the patterned surface. The region for sampling and measurement is divided into small bins along the x and z directions. In both the static and dynamic states, the average molecular densities ρ_1 and ρ_2 for the two fluids are measured to locate the interface (by the condition $\rho_1=\rho_2$, i.e., $\phi=0$). From the time evolution of interface, the velocity of the moving contact line is calculated by differentiating the contact line position with respect to time.

In accordance with the continuum model, the properties of each solid surface (a, b, or c), physically determined by the corresponding intermolecular fluid-solid interactions, can be specified by two slip lengths (for the two fluids) and a static contact angle (defined on the side of fluid B). Given the fluid-solid interaction for one fluid at one solid surface, the slip length can be measured from non-equilibrium MD simulations in single-phase Couette-flow geometry [39]. Given the fluid-solid interactions for two fluids at one solid surface, the static contact angle can be measured from equilibrium MD simulations, as illustrated in Fig. 4. Results from various MD measurements are listed in Table 1. It is seen that larger slip length is associated with less attractive fluid-solid interaction (smaller $\delta_{\alpha\beta}$ parameter) [32]. The shear viscosity $\eta=2.0\sqrt{\epsilon m}/\sigma^2$ and the fluid-fluid interfacial tension $\gamma=4.75\epsilon/\sigma^2$ are also measured for the continuum modeling and simulation.

Table 1: Static contact angles and slip lengths measured from MD simulations for continuum hydrodynamic calculations. In our MD simulations, the parameters $\delta_{\alpha\beta}$ are set to ensure that the fluid A is more attracted to the A-like stripe than the fluid B is while the fluid B is more attracted to the B-like stripe than the fluid A is. To reduce the number of independent parameters, $\delta_{Aa}=\delta_{Bb}$ and $\delta_{Ab}=\delta_{Ba}$ are also assumed. Consequently, we have $\theta_s^b<90^o$, $\theta_s^a=180^o-\theta_s^b$, $l_{sA}^a=l_{sB}^b$, $l_{sA}^b=l_{sB}^a$ as used in continuum calculations. The two fluids have the same interaction with the top wall, i.e., $\delta_{Ac}=\delta_{Bc}$, and hence $\theta_s^c=90^o$ and $l_{sA}^c=l_{sB}^c$.

Parameters for MD simulations	Parameters for continuum calculations
$\delta_{Aa}=0.7,\delta_{Ab}=0.2,\delta_{Ac}=0.7$	$\theta_s^b\approx 57^o, l_{sA}^a\approx 1.9\sigma, l_{sA}^b\approx 14.3\sigma, l_{sA}^c\approx 1.9\sigma$
$\delta_{Aa}=0.8,\delta_{Ab}=0.2,\delta_{Ac}=0.8$	$\theta_s^b\approx 47^o, l_{sA}^a\approx 1.2\sigma, l_{sA}^b\approx 14.3\sigma, l_{sA}^c\approx 1.2\sigma$
$\delta_{Aa}=0.7,\delta_{Ab}=0.3,\delta_{Ac}=0.5$	$\theta_s^b\approx 66^o, l_{sA}^a\approx 1.9\sigma, l_{sA}^b\approx 10.3\sigma, l_{sA}^c\approx 4.6\sigma$

4 Continuum hydrodynamic calculations and comparison with MD simulations

In continuum calculations, we use $\xi=\sigma/3$ as the length unit, $V=0.25\sqrt{\epsilon/m}$ as the velocity unit, and $\eta V/\xi^2$ as the force density unit. We can measure in MD simulations the number density ρ, the shear viscosity η, the interfacial tension γ, the static contact angle, and the slip length. As for the two phenomenological parameters M and Γ, we use $M=0.023\sigma^4/\sqrt{m\epsilon}$ and $\Gamma=0.66\sigma/\sqrt{m\epsilon}$, values optimized for earlier comparison of continuum and MD results [16, 18]. With $\phi_\pm=\pm\sqrt{r/u}=\pm 1$ and $\gamma=2\sqrt{2}r^2\xi/3u$, six dimensionless parameters appear in the continuum model: $\mathcal{L}_d=Mr/\xi V=4.17$, $\mathcal{R}=m\rho\xi V/\eta=0.0338$, $\mathcal{B}=r^2\xi/u\eta V=10.1$, $\mathcal{V}_s=K\Gamma/V=4.43$, the static contact angle θ_s, and the dimensionless slip length $\mathcal{L}_s=l_s/\xi=\eta/\beta\xi$. The two fluid phases may have different interactions with the solid, and hence the slip coefficient β may vary with ϕ at surface. For a particular solid surface (one of the three different solid surfaces, a, b or c), we use $\beta(\phi)=(1-\phi)\beta_1/2+(1+\phi)\beta_2/2$ with ϕ varying between -1 and $+1$ across the fluid-fluid interface. Here β_1 and β_2 are the slip coefficients for the two fluid phases (with $\phi=\pm 1$) on that surface, to be obtained from the slip lengths measured in MD simulations. In their dimensionless forms, Eqs. (2.2), (2.3), (2.4), and (2.5) become

$$\frac{\partial\phi}{\partial t}+\mathbf{v}\cdot\nabla\phi=\mathcal{L}_d\nabla^2(-\nabla^2\phi-\phi+\phi^3), \tag{4.1}$$

$$\mathcal{R}\left[\frac{\partial\mathbf{v}}{\partial t}+(\mathbf{v}\cdot\nabla)\mathbf{v}\right]=-\nabla p+\nabla^2\mathbf{v}+\mathcal{B}(-\nabla^2\phi-\phi+\phi^3)\nabla\phi+\mathbf{f}_e, \tag{4.2}$$

$$\frac{\partial\phi}{\partial t}+v_x\partial_x\phi=-\mathcal{V}_s\left[\partial_n\phi-\frac{\sqrt{2}}{3}\cos\theta_s s_\gamma(\phi)\right], \tag{4.3}$$

$$[\mathcal{L}_s(\phi)]^{-1}v_x^{slip}=-\partial_n v_x+\mathcal{B}\left[\partial_n\phi-\frac{\sqrt{2}}{3}\cos\theta_s s_\gamma(\phi)\right]\partial_x\phi, \tag{4.4}$$

with $s_\gamma(\phi)=(\pi/2)\cos(\pi\phi/2)$. These equations show explicitly the dimensionless parameters in control of the hydrodynamic behaviors. We use a pressure-Poisson solver

for the Navier-Stokes equation and a semi-implicit scheme for the diffusion equation. For direct comparison with the MD results, the continuum results will be presented in the reduced units defined from the Lennard-Jones energy scale ϵ, length scale σ and the molecular mass m.

Continuum calculations are carried out for an immiscible two-phase fluid flowing through a slit pore with homogeneous top surface and patterned bottom surface. We consider two driving modes: (i) The flow is driven by applying an external force density $\mathbf{f}_e = f_e\hat{\mathbf{x}}$ along the x direction. This is for direct comparison with results from MD simulations in which an external force $mg\hat{\mathbf{x}}$ is applied to each fluid molecule. (ii) The flow is driven by imposing an average displacement velocity U along the x direction. This is the driving mode we used in [30]. For either driving mode, appropriate velocity boundary conditions are applied at the left and right boundaries of the channel in the computational domain. They are given by the Poiseuille-type quadratic profile $v_x(z)$, satisfying

$$\partial_z^2 v_x + f_e = 0$$

for the first mode or

$$-\partial_x p + \partial_z^2 v_x = 0 \quad \text{with} \quad \int_0^H dz v_x(z) = UH$$

for the second mode, and is consistent with the slip boundary conditions at the top and bottom surfaces.

It is worth emphasizing that, for contact-line motion at patterned surfaces, the comparison of continuum and MD results can no longer be made for stationary states in which the continuum hydrodynamic variables, e.g., ϕ and $\mathbf{v}$, are time-independent. Instead, the stick-slip motion of the moving contact line requires such comparison to be done for transient states in which the fluid-fluid interface takes oscillatory shape while the contact line moves at oscillatory velocity. Technically, in order to resolve the time evolution in continuum hydrodynamics, the time averaging in MD simulations has to be performed within time intervals that are short enough compared to the characteristic time scales shown in the continuum solutions. To further remove the statistical fluctuations, we also average the velocity and density variables over an ensemble of similar systems, generated by a series of simulations consistent with the "macroscopic" restraints.

For the results presented in Section 5, each interface profile is obtained by averaging over 1τ (i.e., 1000 time steps) because the moving interface only covers a very small distance in this short time interval. Each contact line position is also obtained by averaging over 1τ. Contact line positions at different times are recorded every 2τ. Differentiating the contact line position with respect to time yields the contact line velocity. Ensemble averaging over 10 to 30 systems is employed to reduce the statistical fluctuations, with each system prepared using a very small random perturbation at the initial time. In particular, we have 10 to 30 sets of data in obtaining the contact line velocity as a function of the contact line position. With each pattern period λ divided into many narrow segments, each of 0.5σ along x, the contact line velocities measured within a narrow segment are

collected from different systems and then averaged. This gives the contact line velocity in the middle of that segment.

5 Results and discussion

Now we present the numerical results of both continuum hydrodynamic calculations and MD simulations. The remarkable agreement between the continuum and MD results affirms the stick-slip motion of moving contact line at patterned surfaces, from which a special scaling relation is derived for energy dissipation [30]. From extensive continuum calculations, we also study the physical mechanism controlling the contact-line slip and fluid-fluid interface relaxation.

5.1 Stick-slip motion of moving contact line

5.1.1 Comparison of continuum and MD results

Comparison of continuum and MD results is made for Poiseuille flows driven by external force. Here we start from patterned surfaces of large period. Figs. 5 and 6 show the variations of fluid-fluid interface and contact line velocity along the patterned surface (at the bottom of the channel). For the large period used here ($\lambda = 80\sigma$), it is observed that the fluid-fluid interface moves with constant shape and velocity when it is away from the boundaries between different stripes. Close to each of these boundaries, however, the contact line shows a fast variation in velocity, either a sharp increase followed by a decrease or a sharp decrease followed by an increase. As a consequence, the contact line is forced into an intermittent stick-slip motion by the patterned surface. It is readily seen that the fast variation of contact line velocity is always accompanied by the adjustment in shape of fluid-fluid interface when it crosses a boundary between two different stripes. Therefore, the stick-slip motion arises from the contrast in wetting property (i.e., static contact angle) between the two different types of stripes. Although it is relatively hard to suppress statistical fluctuations in measuring transient behaviors in MD simulations, we have excellent agreement between the continuum and MD results, from interface shape to contact line velocity, down to molecular length scales (a few molecular diameters).

To display the stick-slip motion, the contact line velocity v is plotted as a function of the contact line position x in Figs. 5 and 6. This is to show how v varies along the patterned surface, e.g., where the velocity extrema take place in space. From v as a function of x, it is ready to obtain x as a function of time t, by integrating $dt = dx/v$.

5.1.2 Scaling for energy dissipation: MD evidences

The fluid-fluid interface has to adjust its shape when crossing a boundary between two different stripes, a direct consequence of the switch of static contact angle (illustrated in Fig. 2). The stick-slip motion of contact line results from such periodic shape adjustment. As the origin lies in the switch of an *equilibrium* wetting property, it is expected that the

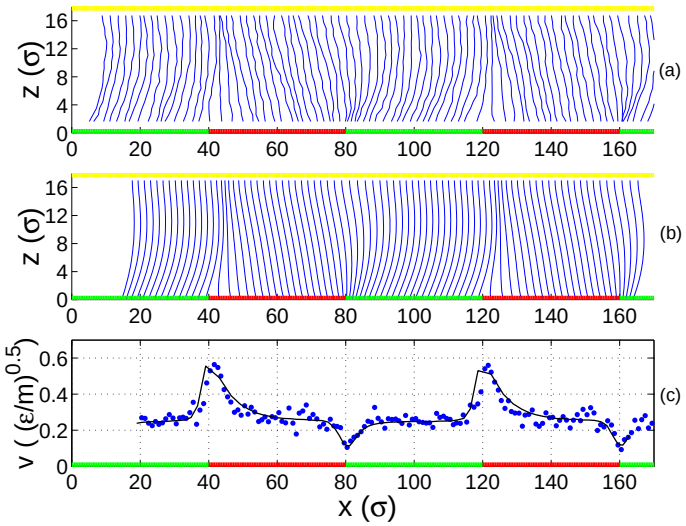

Figure 5: (a) Moving fluid-fluid interface in MD simulation. The time interval between two neighboring interfaces is 8τ. (b) Moving fluid-fluid interface in continuum calculation. The time interval between two neighboring interfaces is 7τ. (c) Contact line velocity at the lower patterned surface, plotted as a function of the contact line position, with symbols for MD results and line for continuum results. The parameters used for interaction potentials are $\delta_{Aa}=\delta_{Bb}=\delta_{Ac}=\delta_{Bc}=0.7$ and $\delta_{Ab}=\delta_{Ba}=0.2$. The external force on each fluid molecule is $mg=0.015\epsilon/\sigma$. The distance between the bottom and top walls is $H=17\sigma$. The pattern period is $\lambda=80\sigma$ with $\lambda_a=\lambda_b$.

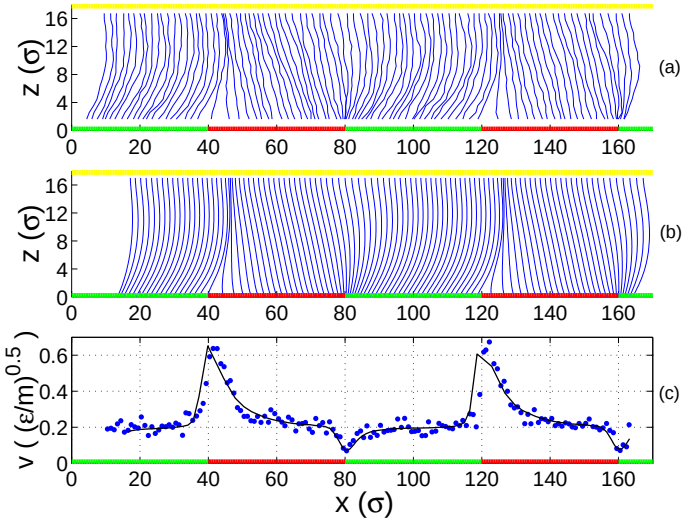

Figure 6: Same as for Fig. 5 except that the parameters used for interaction potentials are $\delta_{Aa}=\delta_{Bb}=\delta_{Ac}=\delta_{Bc}=0.8$ and $\delta_{Ab}=\delta_{Ba}=0.2$. Compared to Fig. 5, the contact line velocity is reduced in the "plateau" region due to the reduced slip lengths (e.g., l^a_{sA} and l^c_{sA}, see Table 1). The peak of the velocity, however, is increased because of the increased difference in static contact angle between the two different types of stripes, from $\theta^b_s=57^o$ and $\theta^a_s=180^o-\theta^b_s$ to $\theta^b_s=47^o$ and $\theta^a_s=180^o-\theta^b_s$ (see Table 1).

stick-slip motion would persist for vanishingly small driving force or average displacement velocity, as shown by our earlier continuum calculations [30]. Here we present results from MD simulations to show the limiting behavior of stick-slip contact line motion. Fig. 7 shows the MD and continuum results for contact line velocity for three different driving forces. Besides their remarkable agreement, it is seen that, as the driving force is continuously reduced, the velocity in the plateau region is also reduced. (Theoretically, the plateau velocity is proportional to the driving force if the stripes are wide enough.) Meanwhile, the dip in velocity (as the interface moves from the A-like stripe to the B-like one) becomes shallower. However, the velocity peak, which appears as the interface moves from the B-like stripe to the A-like one, persists. In particular, the height of the peak, defined as the difference between the maximum velocity and the plateau velocity, actually approaches a constant as the driving force approaches zero. Therefore, in the limit of zero driving force or average displacement velocity, the contact line velocity is everywhere close to zero except around the boundaries where the interface moves from the B-like stripe to the A-like one.

For an immiscible two-phase flow over a homogeneous surface with a steady displacement velocity U, the rate of energy dissipation scales as U^2 for small U, following the general rule governing the entropy production in irreversible thermodynamic processes. On patterned surfaces, however, the fluid-fluid interface undergoes a periodic stick-slip movement with an oscillatory shape, from which extra dissipation arises inevitably. Based on the limit of stick-slip motion shown above, the extra dissipation acquires an unconventional scaling with the average displacement velocity. For slow flows on surfaces patterned with wide stripes, the rate of energy dissipation still scales as U^2 in the plateau region of velocity (away from the boundaries between different stripes). The contribution to time-integrated dissipation over a time period T scales as $U^2T=U^2(\lambda/U)$, which is linear in U. On the other hand, the stick-slip motion has been shown to be independent of U as $U\to 0$. Therefore, the time-integrated extra dissipation incurred by the fluid-fluid interface crossing a boundary is independent of the average displacement velocity. Comparing the above two contributions to time-integrated dissipation, we see that the extra dissipation dominates. As a consequence, the time-averaged rate of energy dissipation is linear in the average displacement velocity for slow flows.

5.1.3 Suppressed stick-slip motion: Approach to homogeneous surface

The numerical results presented above are obtained for patterned surfaces of large period. Over each stripe, the interface moves steadily when it is sufficiently away from the two boundaries of that stripe. When a boundary is crossed, however, the interface has to adjust its shape due to the sudden change of static contact angle, an equilibrium property that can be locally defined. This adjustment in shape is fully manifested in slow flows on surfaces patterned with wide stripes, which allow a full relaxation of fluid-fluid interface. As shown in Section 5.1.2, the time scale associated with the full interfacial relaxation is well defined in the limit of slow flows and wide stripes. When the pattern period is made smaller and/or the interface displacement is made faster, the time for

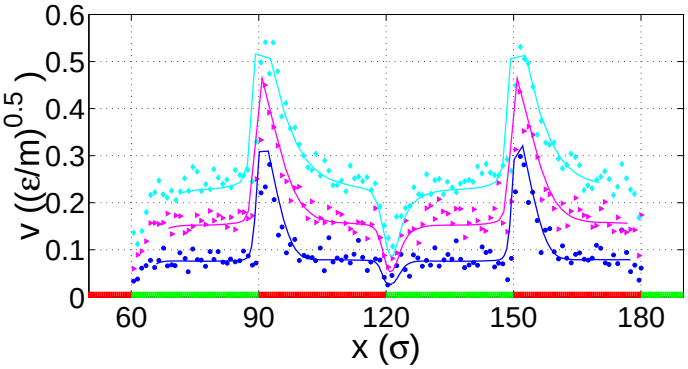

Figure 7: Contact line velocity at the lower patterned surface, plotted as a function of the contact line position, with symbols for MD results and lines for continuum results. The parameters used for interaction potentials are $\delta_{Aa}=\delta_{Bb}=\delta_{Ac}=\delta_{Bc}=0.7$ and $\delta_{Ab}=\delta_{Ba}=0.2$. The external force on each fluid molecule is $mg=0.015\epsilon/\sigma$ (diamond, cyan), $0.01\epsilon/\sigma$ (triangle, magenta), and $0.005\epsilon/\sigma$ (circle, blue). The distance between the bottom and top walls is $H=17\sigma$. The pattern period is $\lambda=60\sigma$ with $\lambda_a=\lambda_b$.

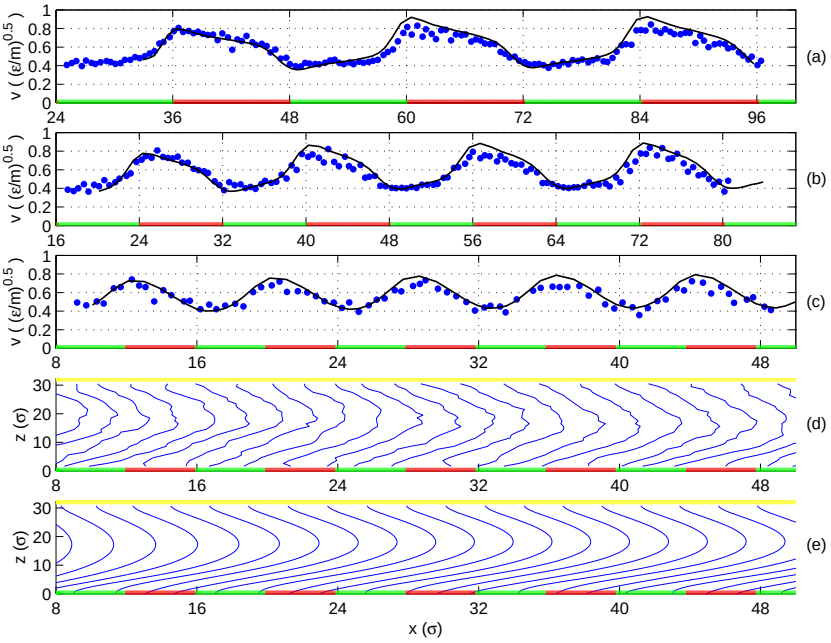

Figure 8: (a) Contact line velocity at the lower patterned surface, plotted as a function of the contact line position, with symbols for MD results and line for continuum results. The parameters used for interaction potentials are $\delta_{Aa}=\delta_{Bb}=0.7$, $\delta_{Ab}=\delta_{Ba}=0.3$, and $\delta_{Ac}=\delta_{Bc}=0.5$. The external force on each fluid molecule is $mg=0.012\epsilon/\sigma$. The distance between the bottom and top walls is $H=30.8\sigma$. The pattern period is $\lambda=24\sigma$ with $\lambda_a=\lambda_b$. (b) Same as for (a) except that the pattern period is $\lambda=16\sigma$. (c) Same as for (a) except that the pattern period is $\lambda=8\sigma$. (d) Moving fluid-fluid interface from the MD simulation for (c). The time interval between two neighboring interfaces is 4τ. (e) Moving fluid-fluid interface from the continuum calculation for (c). The time interval between two neighboring interfaces is 3.6τ.

the interface to cover a period may become smaller than the interfacial relaxation time. As a consequence, the interface can only partially respond to the change of static contact angle when displaced along the patterned surface. If such partial response is further suppressed, then the interface moves as if over an almost homogeneous surface with nearly constant velocity and shape. According to [30], an effective contact angle θ_s^e can be introduced in this limit in the form of

$$\cos\theta_s^e = (\lambda_a/\lambda)\cos\theta_s^a + (\lambda_b/\lambda)\theta_s^b,$$

which means it is the Cassie contact angle. Using both the MD and continuum results with remarkable agreement, Fig. 8 shows the approach to an effectively homogeneous surface as the pattern period is reduced. It is seen that the amplitude of velocity oscillation decreases with decreasing period. Moreover, the interface shape changes very little when the pattern period is small enough. Note that a relatively large distance $H=30.8\sigma$ (compared to $H=17\sigma$ before) has been used to make the interfacial relaxation slower and thus the approach to homogeneous surface easier. Our numerical results (not presented here) also show that, if the pattern period is fixed, then the suppressed oscillation in both contact line velocity and interface shape can be achieved as well through accelerated interface displacement.

5.2 Relaxational dynamics of fluid-fluid interface

The results presented in Section 5.1 have demonstrated the fundamental importance of the time scale associated with the full interfacial relaxation in slow flows over surfaces patterned with wide stripes. The other time scale is that required for the interface to cover a period along the patterned surface. If the latter is much larger than the former, then the interfacial relaxation can be fully manifested, as seen from the fast ascent and more importantly the slow descent of contact line velocity in Fig. 7. If the latter time scale is made smaller than the former (e.g., by shortening the period), then the interfacial relaxation is suppressed and the surface is effectively homogenized. Below we present the numerical results from continuum calculations to investigate the relaxational dynamics of fluid-fluid interface with a focus on its time scale. Here the system setup is a bit different from above, using two identical patterned surfaces for the two walls [30].

To reveal the relaxational nature of the slow descent of contact line velocity in Fig. 7, we plot in Fig. 9(a) the contact line velocity $v_{\rm CL}=\dot{x}_{\rm CL}$ as a function of the contact line position $x_{\rm CL}$ for a very slow flow (the dimensionless average displacement velocity set at $U=-0.0075$). It is readily seen that in approaching the final equilibrium contact line position x_0, the contact line velocity $v_{\rm CL}$ is proportional to the distance $x_{\rm CL}-x_0$. Note that because of the finite value of U, the contact line is always moving and thus has no real equilibrium position. However, here U is extremely small, and hence the displacement due to U is negligible over the time scale $T_{\rm rel}$ of interfacial relaxation. This leads to an "equilibrium" position of contact line with negligible uncertainty, as clearly exhibited in Fig. 9(a).

That $v_{CL}=\dot{x}_{CL}$ is proportional to $x_{CL}-x_0$ shows the approach to x_0 to be exponential in time:

$$x_{CL}-x_0 \propto e^{-t/T_{rel}},$$

in which $1/T_{rel}$, the inverse of relaxation time, can be directly measured from the (nearly constant) slope in Fig. 9(a). To investigate the physical mechanism controlling the interfacial relaxation, we have carried out extensive continuum calculations, seeking the dependence of T_{rel} on those dimensionless parameters listed in Section 4. The major finding is the following. With $\mathcal{L}_d=5$, $\mathcal{R}=0.03$, $\mathcal{V}_s=5$, $\mathcal{L}^a_{sA}=l^a_{sA}/\xi=3.8$, and $\mathcal{L}^b_{sA}=l^b_{sA}/\xi=10$ all fixed (close to the parameter values used for comparison with MD results, see Section 4), the relaxation time T_{rel} is inversely proportional to the dimensionless parameter $\mathcal{B}=r^2\xi/u\eta V$, as shown in Fig. 9(b). According to $\gamma=2\sqrt{2}r^2\xi/3u$ for the interfacial tension, we have $2\sqrt{2}\mathcal{B}/3=\gamma/\eta V$. Therefore, the relaxation time T_{rel} is proportional to $\eta V/\gamma$, the capillary number with V the velocity unit used in de-dimensionalizing the system. To go from the dimensionless T_{rel} to the dimensional one, we note that the time unit is ξ/V. Therefore, the (dimensional) relaxation time T_{rel} is actually proportional to $(\eta V/\gamma)(\xi/V)=\eta\xi/\gamma$. Physically, the interfacial thickness ξ can't be the length scale controlling T_{rel}. The discussion below indicates that the length scale in control is actually the distance between the two walls H, in agreement with the numerical results.

To explain why T_{rel} is proportional to $\eta V/\gamma$, we consider an overdamped system described by one single variable q [20] and governed by the Onsager principle of minimum energy dissipation (entropy production) [22,23]. The equation of motion $\nu\dot{q}=-dF(q)/dq$ can be obtained by minimizing

$$\Phi(\dot{q},\dot{q})+\dot{F}(q,\dot{q})=\nu\dot{q}^2/2+(dF/dq)\dot{q}$$

with respect to $\dot{q}$. Here $\dot{q}$ is the rate corresponding to q, ν is the damping coefficient, $F(q)$ is the free energy function, $\Phi(\dot{q},\dot{q})=\nu\dot{q}^2/2$ is the dissipation function (defined as half the rate of energy dissipation) quadratic in $\dot{q}$, and $\dot{F}(q,\dot{q})=(dF/dq)\dot{q}$ is the rate of change of the free energy. The above equation of motion describes the balance of two forces, one originating from the free energy while the other from the energy dissipation. Physically, the variational principle of minimum energy dissipation yields the most probable course of a dissipative process as long as the displacement from equilibrium is small.

The present system is overdamped (with negligible inertia effect), but the number of degrees of freedom is infinite. Nevertheless, for the linear relation between T_{rel} and $\eta V/\gamma$, we may simply consider one variable only — the contact line position x_{CL}. That is, the rate of total energy dissipation is assumed to be quadratic in $\dot{x}_{CL}$ while the total free energy is assumed to be a function of x_{CL}. Moreover, the free energy is quadratic in $x_{CL}-x_0$ (up to a constant) as $x_{CL}-x_0\to 0$. (This condition for quadratic approximation is better satisfied for smaller contrast in wettability, i.e., θ^b_s closer to 90^o, which leads to a shorter distance traversed by the contact line.) A simple dimension analysis gives the dissipation function (per unit length along the y direction) in the form of $\frac{1}{2}c_1\eta\dot{x}^2_{CL}$ and the free energy (per unit length along the y direction) in the form of $\frac{1}{2}c_2\gamma(x_{CL}-x_0)^2/H$,

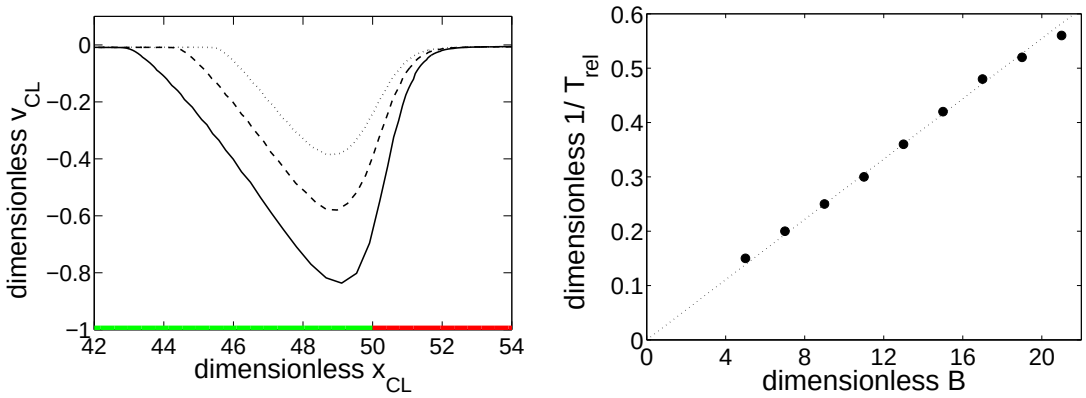

Figure 9: (a) Contact line velocity plotted as a function of contact line position, obtained using the dimensionless parameters $\mathcal{L}_d=5$, $\mathcal{R}=0.03$, $\mathcal{B}=5$, $\mathcal{V}_s=5$, $\mathcal{L}^a_{sA}=l^a_{sA}/\xi=3.8$, and $\mathcal{L}^b_{sA}=l^b_{sA}/\xi=10$. The channel has $H=40$ and $\lambda=100$ with $\lambda_a=\lambda_b$ (A-like stripe on the right and B-like stripe on the left, separated by $x=50$). The three lines are for three different static contact angles: $\theta^b_s=65^o$ (dotted), 60^o (dashed), and 54^o (solid). In approaching the final equilibrium contact line position x_0, the contact line velocity $v_{\rm CL}$ is proportional to the distance $x_{\rm CL}-x_0$. The inverse of relaxation time is measured from the slope in this linear regime. (b) $1/T_{\rm rel}$ plotted as a function of $\mathcal{B}$, with all the other parameters fixed (for $\theta^b_s=65^o$). The dotted line indicates $1/T_{\rm rel}\propto\mathcal{B}$.

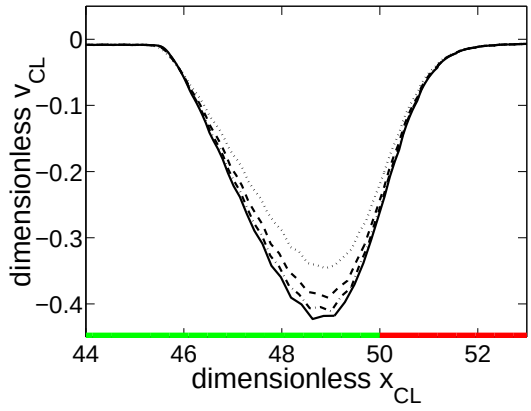

Figure 10: Contact line velocity plotted as a function of contact line position, obtained using the dimensionless parameters $\mathcal{L}_d=5$, $\mathcal{R}=0.03$, $\mathcal{B}=5$, $\mathcal{V}_s=5$, and $\theta^b_s=65^o$ with $\mathcal{L}^a_{sA}/\mathcal{L}^b_{sA}=0.38$ fixed. The channel has $H=40$ and $\lambda=100$ with $\lambda_a=\lambda_b$ (A-like stripe on the right and B-like stripe on the left, separated by $x=50$). The four lines are for four different slip lengths: $\mathcal{L}^a_{sA}=2$ (dotted), 4 (dashed), 6 (dot-dashed), and 8 (solid). It is seen that $1/T_{\rm rel}$ (absolute value of the slope in the linear regime) increases with increasing slip length.

with c_1 and c_2 being two numeric factors. Note that the distance between the two walls H enters into the free energy expression as the only relevant length scale. (Since the free energy comes from the one fluid-fluid interface and the two fluid-solid interfaces in the channel, it depends on a few parameters only: the static contact angle (through the factor c_2), the interfacial tension γ, the contact line position $x_{\rm CL}$ (through the quadratic term $(x_{\rm CL}-x_0)^2$), and the only length scale H.) Applied to this one-variable system, the

variational principle leads to the balance of the "elastic" force $-c_2\gamma(x_{\rm CL}-x_0)/H$ and the dissipative force $-c_1\eta\dot{x}_{\rm CL}$:

$$c_1\eta\dot{x}_{\rm CL}=-\frac{c_2\gamma}{H}(x_{\rm CL}-x_0),$$

from which $T_{\rm rel}$ is found to be $(c_1/c_2)\eta H/\gamma$. This analysis shows H to be the length scale controlling the magnitude of $T_{\rm rel}$, in agreement with the numerical results. The slope of the line in Fig. 9(b) is measured to be 0.028, i.e., $1/T_{\rm rel}=0.028(3/2\sqrt{2})\gamma/\eta V$ in dimensionless form, from which we obtain $T_{\rm rel}\simeq\eta(34\xi)/\gamma$ in dimensional form, where 34ξ is of the same order of magnitude as $H=40\xi$.

We choose to express the dissipation function as $\frac{1}{2}c_1\eta\dot{x}_{\rm CL}^2$ considering that viscous dissipation in the bulk dominates among the four physically distinct sources of dissipation: the shear viscosity in the bulk, the fluid slipping at the solid surface, the composition diffusion in the bulk, and the composition relaxation at the solid surface [30]. The numeric factor c_1 is affected by the contributions of the latter three compared to the viscous one. It has been shown that for the parameters used here, the second largest contribution is from the slipping. Physically, increasing the slip length (i.e., decreasing the slip coefficient) makes the fluid-solid coupling less viscous and hence reduces its contribution to total dissipation. Fig. 10 shows that increasing the slip length can indeed reduce $T_{\rm rel}$ $(\propto c_1)$ by making c_1 smaller. As the fluid slipping only contributes a small part of the total dissipation, the dependence of $T_{\rm rel}$ on the slip length is weak.

6 Concluding remarks

In this paper, we have carried out both continuum calculations and MD simulations to study the stick-slip motion of contact line at chemically patterned surfaces, with remarkable agreement between the continuum and MD results. Such agreement is attributed to the accurate description down to molecular scale by the generalized Navier boundary condition in our continuum model. The fact that our continuum model can reproduce the results of numerical experiments (MD simulations) should not be a surprise from the point of view that by requiring the continuum hydrodynamics to be consistent with the same statistical mechanical principle as that underlying molecular dynamics, the same (time-averaged) dynamic behavior is expected.

Compared with many previous tests of our continuum model in steady states [16, 18, 20], the present problem offers challenges in two different fronts. The first is that the stick-slip motion requires the comparison to be made for transient states with time-varying interface shape and contact line velocity. The second is that the stick-slip motion may involve contact line velocity that is of the same order of magnitude as that of thermal velocity if the difference between the two static contact angles is sufficiently large. The results presented in this paper affirm the validity of our model once again, under the more demanding conditions imposed by the present problem.

Acknowledgments

This publication is based on work partially supported by Award No. SA-C0040/UK-C0016, made by King Abdullah University of Science and Technology (KAUST), Hong Kong RGC grant CA05/06.SC01, and the Croucher Foundation Grant Z0138. T. Qian was also supported by Hong Kong RGC grant No. 602007.

References

[1] G. K. Batchelor, An Introduction to Fluid Dynamics. Cambridge University Press, 1967.
[2] C. Huh and L. E. Scriven, Hydrodynamic model of steady movement of a solid/liquid/fluid contact line. J. Colloid Interface Sci. 35, 85-101, 1971.
[3] E. B. Dussan V. and S. H. Davis, On the motion of a fluid-fluid interface along a solid surface. J. Fluid Mech. 65, 71-95, 1974.
[4] E. B. Dussan V., On the spreading of liquids on solid surfaces: Static and dynamic contact lines. Annu. Rev. Fluid Mech. 11, 371-400, 1979.
[5] J. Koplik, J. R. Banavar and J. F. Willemsen, Molecular dynamics of Poiseuille flow and moving contact lines. Phys. Rev. Lett. 60, 1282-1285, 1988.
[6] P. A. Thompson and M. O. Robbins, Simulations of contact-line motion: Slip and the dynamic contact angle. Phys. Rev. Lett. 63, 766-769, 1989.
[7] T. D. Blake and J. M. Haynes, Kinetics of liquid/liquid displacement. J. Colloid Interface Sci. 30, 421-423, 1969.
[8] L. M. Hocking, A moving fluid interface. Part 2. The removal of the force singularity by a slip flow. J. Fluid Mech. 79, 209-229, 1977.
[9] C. Huh and S. G. Mason, The steady movement of a liquid meniscus in a capillary tube. J. Fluid Mech. 81, 401-419, 1977.
[10] R. G. Cox, The dynamics of the spreading of liquids on a solid surface. Part 1. Viscous flow. J. Fluid Mech. 168, 169-194, 1986.
[11] M. Y. Zhou and P. Sheng, Dynamics of immiscible-fluid displacement in a capillary tube. Phys. Rev. Lett. 64, 882-885, 1990.
[12] P. Seppecher, Moving contact lines in the Cahn-Hilliard theory. Int. J. Eng. Sci. 34, 977-992, 1996.
[13] H. Y. Chen, D. Jasnow and J. Vinals, Interface and contact line motion in a two phase fluid under shear flow. Phys. Rev. Lett. 85, 1686-1689, 2000.
[14] D. Jacqmin, Contact-line dynamics of a diffuse fluid interface. J. Fluid Mech. 402, 57-88, 2000.
[15] A. J. Briant and J. M. Yeomans, Lattice Boltzmann simulations of contact line motion. II. Binary fluids. Phys. Rev. E 69, 031603, 2004.
[16] T. Z. Qian, X. P. Wang and P. Sheng, Molecular scale contact line hydrodynamics of immiscible flows. Phys. Rev. E 68, 016306, 2003.
[17] J. W. Cahn and J. E. Hilliard, Free energy of a nonuniform system. I. Interfacial free energy. J. Chem. Phys. 28, 258-267, 1958.
[18] T. Z. Qian, X. P.Wang, and P. Sheng, Power-law slip profile of the moving contact line in two-phase immiscible flows. Phys. Rev. Lett. 93, 094501, 2004.
[19] T. Z. Qian, X. P. Wang, P. Sheng, Molecular hydrodynamics of the moving contact line in two-phase immiscible flows. Comm. Comput. Phys. 1, 1-52, 2006.

[20] T. Z. Qian, X. P. Wang, P. Sheng, A variational approach to moving contact line hydrodynamics. J. Fluid Mech. 564, 333-360, 2006.
[21] T. Z. Qian, X. P. Wang, P. Sheng, A scaling approach to the derivation of hydrodynamic boundary conditions. J. Fluid Mech. 611, 333-364, 2008.
[22] L. Onsager, Reciprocal relations in irreversible processes. I. Phys. Rev. 37, 405-426, 1931.
[23] L. Onsager, Reciprocal relations in irreversible processes. II. Phys. Rev. 38, 2265-2279, 1931.
[24] H. Gau, S. Herminghaus, P. Lenz and R. Lipowsky, Liquid morphologies on structured surfaces: From microchannels to microchips. Science 283, 46-49, 1999.
[25] A. A. Darhuber, S. M. Troian, S. M. Miller and S. Wagner, Morphology of liquid microstructures on chemically patterned surfaces. J. Appl. Phys. 87, 7768-7775, 2000.
[26] T. Cubaud and M. Fermigier, Advancing contact lines on chemically patterned surfaces. J. Colloid Interface Sci. 269, 171-177, 2004.
[27] O. Kuksenok, D. Jasonw, J. Yeomans and A. Balazs, Periodic droplet formation in chemically patterned microchannels. Phys. Rev. Lett. 91, 108303, 2003.
[28] H. Kusumaatmaja, J. Leopoldes, A. Dupuis and J. M. Yeomans, Drop dynamics on chemically patterned surfaces. Europhys. Lett. 73, 740-746, 2006.
[29] W. Ren and W. E, Boundary conditions for the moving contact line problem. Phys. Fluid 19, 022101, 2007.
[30] X. P. Wang, T. Z. Qian and P. Sheng, Moving contact line on chemically patterned surfaces. J. Fluid Mech. 605, 59-78, 2008.
[31] R. Chella and J. Vinals, Mixing of a two-phase fluid by cavity flow. Phys. Rev. E 53, 3832-3840, 1996.
[32] J.-L. Barrat and L. Bocquet, Large slip effect at a nonwetting fluid-solid interface. Phys. Rev. Lett. 82, 4671-4674, 1999.
[33] J. R. Philip, Integral properties of flows satisfying mixed no-slip and no-shear conditions. Z. Angew. Math. Phys. 23, 960-968, 1972.
[34] E. Lauga and H. A. Stone, Effective slip in pressure-driven Stokes flow. J. Fluid Mech. 489, 55-77, 2003.
[35] C. Cottin-Bizonne, J.-L. Barrat, L. Bocquet and E. Charlaix, Low-friction flows of liquid at nanopatterned interfaces. Nat. Mater. 2, 237-240, 2003.
[36] N. V. Priezjev, A. A. Darhuber and S. M. Troian, Slip behaviour in liquid films on surfaces of patterned wettability: Comparison between continuum and molecular dynamics simulations. Phys. Rev. E 71, 041608, 2005.
[37] W. Ren and W. E, Heterogeneous multiscale method for the modeling of complex fluids and micro-fluidics. J. Comput. Phys. 204, 1-26, 2005.
[38] T. Z. Qian, X. P. Wang and P. Sheng, Hydrodynamic slip boundary condition at chemically patterned surfaces: A continuum deduction from molecular dynamics. Phys. Rev. E 72, 022501, 2005.
[39] P. A. Thompson and S. M. Troian, A general boundary condition for liquid flow at solid surfaces. Nature 389, 360-362, 1997.